European Journal of Medicinal Chemistry 79 (2014) 436–445

Contents lists available at ScienceDirect

European Journal of Medicinal Chemistry

journal homepage: http://www.elsevier.com/locate/ejmech

Original article

Synthesis and biological evaluation of novel ^{123}I-labeled 4-(4-iodophenyl)butanoyl-L-prolyl-(2*S*)-pyrrolidines for imaging prolyl oligopeptidase *in vivo*

Annukka Kallinen [a,*], Boyan Todorov [a], Roope Kallionpää [b], Susanne Bäck [c], Mirkka Sarparanta [a], Mari Raki [d], Juan A. García-Horsman [c], Kim A. Bergström [d,e], Erik A.A. Wallén [b], Pekka T. Männistö [c], Anu J. Airaksinen [a,*]

[a] Laboratory of Radiochemistry, Department of Chemistry, P.O. Box 55, FI-00014 University of Helsinki, Finland
[b] Division of Pharmaceutical Chemistry, Faculty of Pharmacy, P.O. Box 56, 00014 University of Helsinki, Finland
[c] Division of Pharmacology and Toxicology, Faculty of Pharmacy, P.O. Box 56, 00014 University of Helsinki, Finland
[d] Centre for Drug Research, Faculty of Pharmacy, P.O. Box 56, 00014 University of Helsinki, Finland
[e] HUS Medical Imaging Center, Helsinki University Central Hospital, Finland

ARTICLE INFO

Article history:
Received 16 October 2013
Received in revised form
2 April 2014
Accepted 4 April 2014
Available online 12 April 2014

Keywords:
^{123}I-radiotracer
Prolyl oligopeptidase
Biodistribution
Inflammation

ABSTRACT

Prolyl oligopeptidase (POP) may be associated with neuromodulation and development of neurodegenerative diseases and it was recently shown to participate in the inflammatory cascade along with matrix metalloproteinases. Radiotracers, which can be used for non-invasive imaging, are needed for investigating the role of POP in normal physiology and in pathophysiological conditions *in vivo*. We synthesized two novel POP-specific ^{123}I-radiolabeled 4-phenylbutanoyl-L-prolyl-pyrrolidines of which 4-(4-[^{123}I]iodophenyl)butanoyl-L-prolyl-2(*S*)-cyanopyrrolidine ([^{123}I]**2f**, K_i = 4.2 nM) was selected. The selected compound has an electrophilic cyano group that is known to increase the dissociation time of POP inhibitors. [^{123}I]**2f** was synthesized in high radiochemical yield and purity (87 ± 4%, >99%, respectively) and with a specific activity of 456 ± 98 GBq/μmol. [^{123}I]**2f** was evaluated in healthy mice (C57Bl/6JRccHsd) by *ex vivo* biodistribution studies and SPECT imaging. Pretreatment with the known inhibitor 4-phenylbutanoyl-L-prolyl-(*2S*)-cyanopyrrolidine (KYP-2047, **2d**, K_i = 0.023 nM) showed that binding of [^{123}I]**2f** was POP specific. In addition, [^{123}I]**2f** was evaluated in models of neuroinflammation and acute localized inflammation. A minor increase in binding of [^{123}I]**2f** was observed in the inflamed region in the acute localized inflammation model. Similar increase in binding was not observed in the neuroinflammation model.

1. Introduction

Prolyl oligopeptidase (POP, also known as prolyl endopeptidase, PREP) (EC 3.4.21.26) is an endopeptidase that hydrolyzes L-proline peptide bonds on the carboxylic acid side of L-proline residue in peptides comprised of a maximum of 30 amino acids. It belongs to a larger prolyl oligopeptidase family S9 which includes enzymes dipeptidyl peptidase IV (DPPIV), acylaminoacyl peptidase and oligopeptidase B [1,2]. Most of the studies indicate that POP is a soluble cytosolic enzyme, although evidence for the existence of a membrane bound form of the enzyme has also been presented [3]. POP has been suggested to have a role in the metabolism of neuropeptides. However, studies with POP inhibitors have ended up with contradicting results, maintaining the role of the enzyme in the metabolism of the neuropeptides elusive. [4,5] Alternatively, POP has been shown to be involved in the cycle of inositol triphosphate (IP_3), a secondary messenger transmitting the receptor-mediated signaling of several neuropeptides [6]. Lately, POP activity has been correlated to an increase in the accumulation of α-synuclein, an insoluble fibrillar inclusion typically found in Parkinson's disease (PD) and in Lewy body dementia [7,8]. Moreover, it was shown very recently that the inhibition of POP resulted in a decrease of α-synuclein accumulation in an α-synuclein-expressing transgenic mouse model [9], and that POP co-localizes

Abbreviations: POP, Prolyl oligopeptidase; PD, Parkinson's disease; MMP, matrix metalloproteinases; LPS, lipopolysaccharide.

* Corresponding authors.
E-mail addresses: annukka.kallinen@helsinki.fi, annukka.kallinen@ansto.gov.au (A. Kallinen), anu.airaksinen@helsinki.fi (A.J. Airaksinen).

http://dx.doi.org/10.1016/j.ejmech.2014.04.014
0223-5234/

with α-synuclein in the brain of PD patients [10]. In the same study it was also shown that POP co-localizes with the tau protein.

Recently, several studies have indicated that POP may have a role in inflammatory diseases [11]. POP has been found in granule-like structures in the cytoplasm of neutrophils [12]. Other studies implicate concerted action of POP and matrix metalloproteinases (MMP) in the degradation of collagen at the site of inflammation. The MMPs degrade the collagen strands thus exposing prolyl-glycyl-proline (PGP) moieties that serve as substrates for POP. The tripeptide PGP, specifically cleaved and released by POP, can subsequently act as a chemoattractant for neutrophils [11]. In multiple sclerosis, an autoimmune disease where matrix metalloproteinases are upregulated, POP activity has been found consistently altered in the forms of the disease with a strong inflammatory component [13]. These findings suggest a rationale for studying the possible involvement of POP in neurodegenerative diseases where an inflammatory component is typically found, and support its possible role as a disease biomarker [14].

In vivo molecular imaging is an important tool in investigation of biological processes and molecular interactions in preclinical animal models. A synthesis and use of a tight-binding fluorescent POP inhibitor for the detection of POP in cell cultures via optical imaging has been reported earlier [15,16]. By using imaging modalities based on distribution of radiolabeled tracer molecules, such as positron emission tomography (PET) and single photon emission computed tomography (SPECT), the preclinical imaging methodology can be readily translated to clinical applications. However, investigation of the role of POP in normal physiology and in pathophysiological conditions, especially in the CNS, has been hampered by the lack of an imaging tracer specific for POP. By developing radiolabeled POP inhibitors for *in vivo* imaging, new information on the localization of the enzyme and its role in neuromodulation and development of neurodegenerative and inflammatory diseases could be obtained. To the best of our knowledge, only one research group has published radiolabeled POP inhibitors. The syntheses of radiolabeled POP inhibitors ((2-(8-(*N*,*N*-([^{11}C]methyl)methylamino)octylthio))-6-isopropyl)-3-pyridyl 2-thienyl ketone ([^{11}C]**1b**, K_i = 0.95 nM, rat brain POP) [17] and *N*-((*N*-(-4-(*N*-[^{11}C]methylamino)phenyl)butyryl)-L-prolyl)pyrrolidine ([^{11}C]**2c**, IC_{50} = 3.1 nM, mouse brain POP) [18] from the corresponding desmethylated precursors **1a** and **2b** (Fig. 1) via ^{11}C-methylation have been described previously, although no biological evaluation of these tracers has been reported [19,20].

To add a new tool for the research on the physiological role of POP, and in search of new diagnostic applications, we decided to synthesize ^{123}I-labeled analogues of **2a** (SUAM-1221) [21] and **2d** (KYP-2047) [22] (Fig. 1) and to investigate the biodistribution in healthy mice with SPECT/CT. The K_i values for **2a** and **2d** are 0.97 nM and 0.023 nM, respectively [23]. Inhibitor **2d** is a slow, tight-binding inhibitor [23], because it forms an imino ether adduct with the enzyme [24]. The long-lasting inhibition would provide a possibility for the signal detection over several hours [23]. The *para*-position of the phenyl ring was chosen as the site for introducing the ^{123}I-label, as different substituents have previously been added to this position without substantial changes in the binding affinity. The aromatic position should also result in a relatively stable radiolabeling, when considering the *in vivo* stability of the final structure.

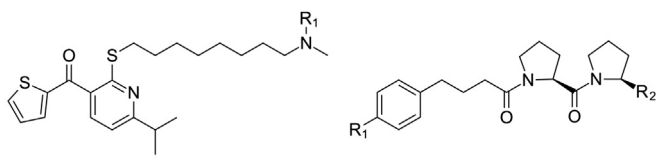

1a (desmethyl Y-29794): R_1 = H
[^{11}C]**1b**: R_1 = $^{11}CH_3$

2a (SUAM-1221): R_1 = H; R_2 = H
2b: R_1 = NH_2; R_2 = H
[^{11}C]**2c**: R_1 = NH[^{11}C]CH_3, R_2 = H
2d (KYP-2047): R_1 = H; R_2 = CN
2e: R_1 = I; R_2 = H
2f: R_1 = I; R_2 = CN

Fig. 1. Structures of POP inhibitors **1a** (desmethyl Y-29794) and **2a** (SUAM-1221) and their radiolabeled derivatives.

In this study we have described the synthesis, radiosynthesis and *in vitro* characterization of the ^{123}I-labeled analogues of POP inhibitors **2a** and **2d**. We have also presented the first evaluation of a radiolabeled POP inhibitor *in vivo* in mice. Considering the possible involvement of POP in inflammation and its potential use as an imaging biomarker for inflammation, we made a preliminary evaluation of the selected radiolabeled POP inhibitor in two animal models of acute inflammation.

2. Results & discussion

2.1. Chemistry

The iodide substituted analogues **2e** and **2f** of the known POP inhibitors **2a** (SUAM-1221) and **2d** (KYP-2047), respectively, were synthesized in good yields following a general synthetic procedure originally reported by Arai et al. (Scheme 1) [22,25].

2.2. Evaluation of the binding properties with in vitro enzyme assay

To determine whether the *p*-iodo-substituent on the phenyl ring affected the inhibitory activity, the apparent K_i values of **2d**, **2e** and **2f** were determined. The obtained values for **2d**, **2e** and **2f** were 0.1, 22 and 4.2 nM, respectively (Fig. 2). These results indicate that the *p*-iodination decreased the inhibitory activity of the compounds, however the constants still are at low nanomolar range. Because of the higher inhibitory potency over **2e**, **2f** was chosen for further *in vitro* characterization and *in vivo* studies.

2.3. Radiochemistry

For the radiosynthesis, **2e** and **2f** were treated with hexamethylditin in the presence of $Pd(PPh_3)_4$-catalyst to give the stannane precursors **5a** and **5b** in 73% and 75% yield, respectively (Scheme 2). The radiosynthetic step was performed according to the methods described in the literature [26]. First, the oxidation was optimized with respect to radiochemical yield and the purity by testing different oxidation agents. The relatively mild oxidant Iodogen® was tested for precursor **5b** resulting in a low radiochemical yield of [^{123}I]**2f** (15%) (Table 1). Chloramine-T (CAT) gave moderate to high radiochemical yields (80–90%), however, an unwanted UV-active side product eluting simultaneously to the tracer was detected in the HPLC purification. The side product may have resulted from the chlorination side reactions often encountered with CAT based oxidants. Lastly, peracetic acid was tested, which resulted in high radiochemical yields (>99%) and purities (>99%) of [^{123}I]**2e** and [^{123}I]**2f** in a small-scale synthesis (radioactivity 10 MBq, 1.14 pmol of ^{123}I). The optimal reaction conditions proved to be the reaction time of 10 min at room temperature in aqueous solution containing 20 equiv of peracetic acid in neutral conditions, and the use of 12 equiv of metabisulphite to quench the oxidant. On the basis of *in vitro* enzyme assay studies, it was decided to continue to *in vivo* evaluation with tracer [^{123}I]**2f** showing a higher affinity to the target enzyme. The optimized reaction conditions were used in a larger scale synthesis with the starting activities ranging from 300 to 680 MBq. [^{123}I]**2f** was obtained with an average radiochemical

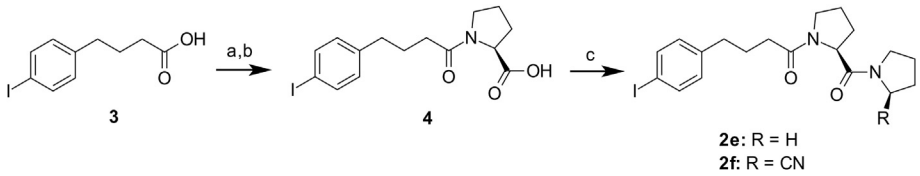

Scheme 1. Synthesis of the stable reference compounds **2e** and **2f**. *Reagents and conditions*: (a) $SOCl_2$, 65 °C, 2 h; (b) L-proline, Na_2CO_3, Et_2O/H_2O, 0 °C → room temperature (74%); (c) for **2e**, 1.) Pivaloyl chloride, TEA, DCM, 0 °C, 1 h, 2.) Pyrrolidine, TEA, DCM, 0 °C → room temperature (81%); for **2f**, 1.) Pivaloyl chloride, DIPEA, DCM, 0 °C, 1 h, 2.) 2(*S*)-cyanopyrrolidine (as TFA salt), DIPEA, DCM, 0 °C → room temperature (57%).

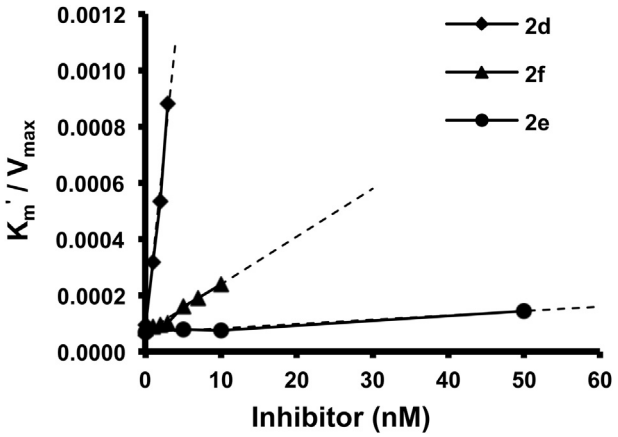

Fig. 2. The kinetic studies of POP inhibition were conducted on the recombinant porcine POP enzyme and the inhibitors **2e**, **2f** and **2d** (KYP-2047). Apparent K_i's were estimated from the intercepts of the dotted lines at the inhibitor concentration axis in this graph. Apparent K_m/V_{max} values were obtained from the reciprocals varying substrate concentrations at the given inhibitor concentrations.

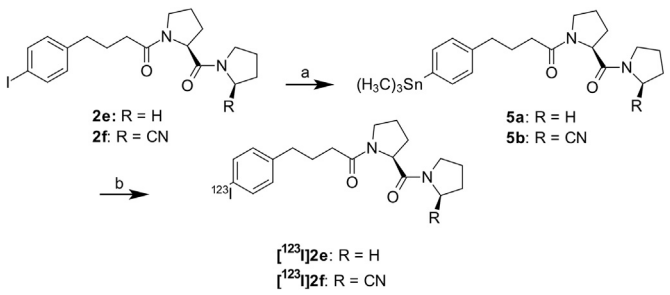

Scheme 2. Radiosynthesis of [^{123}I]**2e** and [^{123}I]**2f**. *Reaction conditions*: (a) hexamethylditin, $PdPPh_4$, toluene (**5a**, 73%; **5b**, 75%); (b) 1. [^{123}I]NaI, peracetic acid (aq), 10 min; 2. $Na_2S_2O_5$ (87 ± 4%, decay corrected yield).

incorporation yield of 82 ± 4% ($n = 4$) and with the radiochemical purity of >99%. The specific activity was 456 ± 98 GBq/μmol at the end of synthesis.

2.4. In vitro stability and LogP

The tracer stability was studied in human plasma at 37 °C up to 120 min (2.5 MBq of tracer/1 mL of plasma). The tracer [^{123}I]**2f** showed excellent stability *in vitro*, no decomposition or radioactive metabolites could be detected by HPLC (system A, method A1). The average amount of 6.3% ± 0.7% of the added radioactivity was found to bind in plasma proteins *in vitro* over 2 h. In the development of CNS radiotracers, moderate lipophilicity (LogP 1.5–2.7) is needed to ensure the passive entry of radiotracer through the BBB into the brain [27]. The LogP value of [^{123}I]**2f** was determined experimentally by the shake flask method [28]. The determined LogP value was 2.37 ± 0.11, indicating a suitable lipophilicity for the passive CNS targeting.

2.5. Biodistribution studies

The biodistribution of [^{123}I]**2f** was investigated in healthy male mice by measuring the radioactivities of selected excised organs at 5, 20, 40, 80 and 160 min post injection, and non-invasively by SPECT-imaging. The overall biodistribution of radioactivity after intravenous injection of [^{123}I]**2f** (2.86 ± 1.26 MBq, 1% DMSO in 0.9% NaCl) in mice in main organs as a function of time is presented in Fig. 3. In the early time points, high accumulation of radioactivity in lungs was seen. The radioactivity in lungs decreased steadily over time, approximately half of the radioactivity being left at 40 min post injection. Organs of moderate radiotracer uptake were heart, kidney, liver and spleen, all of which are reported to have a high expression level of the enzyme in mouse [29,30]. In addition, we found binding in salivary gland and tongue. The uptake in thyroid was initially 52 %ID/g at 5 min timepoint and decreased to 9.4 %ID/g at 160 min ($n = 1$), indicating that relatively little deiodination took place *in vivo*.

Previous studies have demonstrated that POP is widely distributed not only in peripheral tissues but also in brain [30]. The brain uptake of [^{123}I]**2f** remained low over time. The brain uptake of [^{123}I]**2f** was initially 0.43 ± 0.14 %ID at 5 min, increased to 0.76 ± 0.58 %ID at 40 min, and reached a plateau at 80 min (0.27 ± 0.08 %ID) (Fig. 3). The distribution of radioactivity in different brain regions was found to be highly homogenous, which was confirmed by *ex vivo* autoradiography studies (data not shown). Consequently, the brain uptake of [^{123}I]**2f** was found to be insufficient for CNS imaging.

To determine the specific binding of [^{123}I]**2f** to POP *in vivo*, the effect of pretreatment with a known, high-affinity POP-inhibitor **2d** (KYP-2047, $K_i = 0.023$ nM, 50 μmol/kg, 10 mL/kg) [31] on the biodistribution of radioactivity was examined. **2d** was injected intraperitoneally 10 min prior the tracer administration, as described earlier elsewhere [31]. Specific binding could clearly be seen starting from the 40-min time point and it was noted to further enhance during the later time points, indicating faster wash-out from the non-specific binding sites. The results of the study at 80 min post injection are compiled in Table 1. The binding was found to be specific for POP in brain, liver, lung, heart, spleen, muscle, salivary gland ($p \leq 0.05$) and quite surprisingly, in tongue ($t = 160$ min, blocking $p = 0.003$). The higher radioactivity levels in the urine samples indicated an increase in the renal elimination rate after **2d** pretreatment. Accordingly, the increase in the elimination rate of [^{123}I]**2f** after **2d** pretreatment could be clearly seen in the SPECT images as highly active renal and hepatobiliary excretion (Fig. 4).

2.6. Radioactive metabolites of [^{123}I]2f in plasma

Radioactive metabolites of [^{123}I]**2f** were analyzed by HPLC from plasma after i.v. injection of the tracer to mice. A HPLC

Table 1
Biodistribution of [^{123}I]**2f** in C57Bl/6JRccHsd male mice at 80 min in baseline conditions and after pretreatment with **2d** (KYP-2047, 50 μmol/kg, 10 mL/kg, i.p. 10 min prior to the tracer injection).[a]

Organ	80 min control	80 min blocking	Blocking (%)	p[b]
Blood	2.10 ± 0.93	2.69 ± 0.68 (n = 2)	28	nd
Liver	20.10 ± 3.81	5.05 ± 1.69	−75	0.002
Lung	14.67 ± 2.77	1.54 ± 0.46	−89	0.033
Heart	12.20 ± 5.05	1.34 ± 0.38	−89	0.023
Kidney	10.02 ± 4.33	4.73 ± 1.22	−53	0.088
Spleen	10.56 ± 3.26	0.92 ± 0.24	−91	0.036
Testis	0.55 ± 0.18	0.57 ± 0.15	5	0.850
Urine	2.23 ± 2.54	45.24 ± 3.41 (n = 2)	1933	nd
Muscle	2.15 ± 0.60	0.59 ± 0.19	−73	0.010
Salivary gland	7.77 ± 2.21	1.52 ± 0.28	−80	0.010
Tongue	4.43 ± 0.65 (n = 2)	1.44 ± 0.31	−68	nd
Brain	0.62 ± 0.21	0.08 ± 0.02	−88	0.013

[a] Data are expressed as percentage of injected dose per gram ± SD, n = 3.
[b] p-values for the baseline versus blocking group at 80 min post injection by Student's t test (two-tailed, independent).

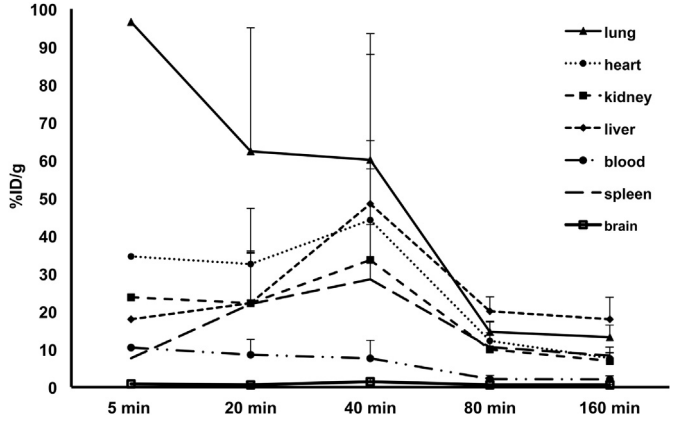

Fig. 3. Biodistribution of radioactivity in an adult C57Bl/6JRccHsd mouse after intravenous injection of [^{123}I]**2f** in selected organs. %ID/g is percentage of injected dose per gram. At 5 min n = 2; at 20, 40 and 160 min n = 3; at 80 min n = 4.

chromatogram of a plasma sample collected at 20 min post injection is shown in Fig. 5A. The activity is presented as a ratio cpm/total cpm. The retention time (t_r) of the parent compound [^{123}I]**2f** varied between 7.15 and 7.80 min. One less lipophilic radioactive metabolite was detected in plasma (t_r = 4 min). The ratio of the parent tracer and the metabolite in blood over time is shown in Fig. 5B (5–40 min, n = 1; 80 and 160 min, n = 2). After 20 min, the observed radioactive metabolite accounted for 61% of the radioactivity found in blood.

We tried to analyze the possible radioactive brain metabolites, however, in the extraction process approximately 70% of the radioactivity was left unextracted in SPE cartridge, compromising the validity of these results. Compounds that have a similar cyanopyrrolidine moiety found in [^{123}I]**2f** structure have been shown to decompose mainly via hydrolysis of the cyano group to a carboxylic acid *in vivo* [32]. The presence of a hydrophilic radiometabolite found in plasma could hence be explained by the cyano group hydrolysis. However, the hydrophilic radiometabolite would not likely enter the brain as readily as the more lipophilic parent tracer.

2.7. Binding to blood components in vivo

We also determined the binding of [^{123}I]**2f** to blood components in mice. The radioactivity in blood and the distribution of radioactivity in blood cells, plasma proteins and free plasma at 20, 40, 80 and 160 min time points are presented in Table 2. Radiotracers that bind avidly to plasma proteins or blood cells have reduced amount of freely available tracer in circulation, and as a consequence, usually show a low brain uptake [33]. The plasma protein bound fraction constituted ~3% of the activity in blood. However, [^{123}I]**2f** was found to partition largely into blood cells; at 20 min, over 90% of the activity in blood resided in the cell fraction. The activity of free, non-protein bound plasma fraction was found to increase over time, at the expense of the decreasing activity in blood cell fraction. The increased activity in the protein-free plasma was mostly due to the accumulation of the main radiometabolite over time. At the 80 min timepoint, the non-bound parent compound accounted only for 0.8% of the activity in blood.

Interestingly, as the selective POP inhibitor **2d** was administered prior to the tracer injection, the activity in blood (%ID/g) was not changed. However, the activity bound to blood cells decreased by 43.5% (at 20 and 160 min), indicating that the binding of the tracer in the blood cells was partly POP specific. In humans, POP has been found in thrombocytes and neutrophils [12,34]. In mice, POP has been found in the peripheral, naive T-cells, although in less amount than in immature thymocytes [35]. It is to be noted though that the binding of [^{123}I]**2f** in blood cells may increase the background signal and hence hinder the use of the tracer for imaging purposes.

2.8. Evaluation of [^{123}I]**2f** for the imaging of POP in the models of acute neuroinflammation and acute localized inflammation

As we were looking into a possibility of using POP as a biomarker for inflammation, we tested the tracer [^{123}I]**2f** in models of acute inflammation in the CNS and in the periphery. Lipopolysaccharide (LPS) induced acute neuroinflammation model [36,37] was chosen for the evaluation of [^{123}I]**2f** as a POP specific tracer for the imaging of neuroinflammation. In the LPS model of neuroinflammation, BBB is reported to be compromised, thus increasing its permeability in both hemispheres [38]. C57Bl/6JRccHsd mice (n = 3) were subjected to stereotaxic injections of LPS in the left striatum 24 h before i.v. injection of [^{123}I]**2f**. The biodistribution of the tracer was studied up to 80 min after tracer injection. The right hemisphere was intact and served as a control in each mouse. In the LPS-induced neuroinflammation model, we did not observe any difference in the uptake of the tracer between the affected (1.34 ± 0.37 %ID/g) and the control hemispheres (1.09 ± 0.38 %ID/g) (Fig. 6A). The overall brain uptake of the radiotracer, however, was noted to increase from 0.27 ± 0.08 %ID to 0.60 ± 0.14 %ID in the LPS-treated mice compared to the healthy mice due to the disrupted BBB, as expected. Although an increase in the POP activity of the neutrophils treated with LPS has been earlier reported [12], there is no previous evidence on the increased POP enzyme levels in the selected animal model. The insufficient binding in the inflamed hemisphere may have been either due to the insensitivity of [^{123}I]**2f** to detect the increased POP enzyme levels in the brain or due to lack of increase in the POP levels in this particular model.

To determine the sensitivity of [^{123}I]**2f** for detection of POP in acute peripheral inflammation, we studied the uptake of [^{123}I]**2f** in the inflamed tissue in turpentine-induced model of acute localized inflammation in C57Bl/6JRccHsd mice (n = 2). The mice were subjected to i.m. injections of turpentine in the right *musculus gastrocnemius* 24 h prior to tracer administration. The left *m. gastrocnemius* was treated with i.m. saline injection as a control. Mice were scanned (60 min) by SPECT-CT at 20 min, 4 h and 24 h after tracer administration, after which the *ex vivo* biodistribution studies were done. In the *ex vivo* studies (timepoint 24 h), we observed a trend of increase in the uptake of [^{123}I]**2f** in the inflamed muscle as compared to the control area (2.0 ± 0.6 %ID/g and

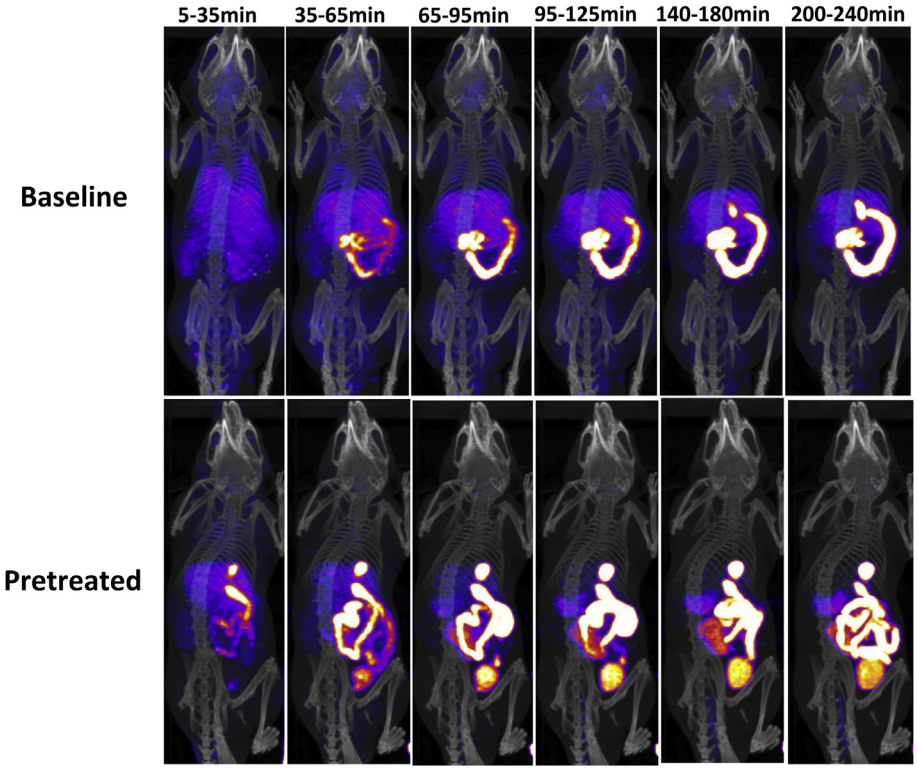

Fig. 4. SPECT-CT images of C57Bl/6JRccHsd male mice after injection of radiotracer [^{123}I]**2f**. Uptake of [^{123}I]**2f** is seen in liver, lungs and in tongue (top row). After pretreatment with a known POP-inhibitor **2d** (KYP-2047) (bottom row), binding of the radiotracer [^{123}I]**2f** in these organs is blocked and the tracer is eliminated faster.

0.8 ± 0.1 %ID/g, respectively) (Fig. 6B). However, the accumulation of the tracer in the inflamed area was clearly not high enough for imaging of inflammation.

3. Conclusions

In vivo imaging of POP with γ-emitting radiotracers offers a new tool for studying the localization and the physiological role of this pharmacologically interesting target. In this study, we successfully synthesized two SPECT radiotracers [^{123}I]**2e** and [^{123}I]**2f** with high radiochemical yields and purities and reported the first biological evaluation of a radiolabeled POP inhibitor. [^{123}I]**2f** showed high inhibitory activity (K_i = 4.2 nM) for the target enzyme and POP specific binding *in vivo*. The slow dissociation of [^{123}I]**2f** from the enzyme would allow a selective detection of the POP protein for several hours. [^{123}I]**2f** is a potential radiotracer for studying peripheral POP levels *in vivo* by using SPECT imaging, however, its insufficient brain uptake hampers its use in assessing changes in the enzyme levels in the brain. Although [^{123}I]**2f** was not successful in the detection of inflammation in the chosen models of inflammation in this preliminary study, the potential of POP enzyme as a possible biomarker and pharmaceutical target certainly deserves further investigation.

4. Experimental section

4.1. General

All chemicals, reagents and solvents for the synthesis of the compounds were analytical grade, purchased from Sigma–Aldrich chemical company (St. Louis, MO, USA) and used without further purification. All air- and moisture-sensitive reactions were performed under argon atmosphere in dry solvents. Flash chromatography was performed on Merck silica gel 60 (0.040–0.063 mm) (Merck, Whitehouse Station, NJ, USA). Thin layer chromatography (TLC) was carried out on silica gel-coated aluminum sheets (Merck, TLC silica gel 60 F_{254}) using solvent mixtures of n-hexane and ethyl acetate. Compounds were visualized by UV-light (254 nm) or by I_2 vapor. Melting points were measured using Büchi 510 melting point apparatus (Büchi Labortechnik AG, Flawil, Switzerland). Optical rotations were determined using wavelength 589 nm at 25 °C by Jasco DIP-1000 polarimeter (Jasco Inc. Mary's Court, MD, USA). NMR spectra were recorded in $CDCl_3$ on Varian 300 MHz (^{1}H NMR, 300 MHz; ^{13}C NMR, 75 MHz) spectrometer (Varian Inc. Palo Alto, CA, USA). TMS (^{1}H) and $CDCl_3$ (^{13}C) were used as internal standards. All recorded spectra were given in ppm (δ). Mass analyses were performed on electrospray ionization mass spectrometer (Bruker Esquire 3000 plus) (Bruker Corporation, Billerica, MA, USA). Microanalyses (C, H, N) were carried out on a VarioMICRO apparatus (Elementar Analysensysteme GmbH, Hanau, Germany). The chemical purities of non-radioactive compounds were ≥95%, unless otherwise stated. The purities were assessed by HPLC and CHN analysis. All HPLC-analyses and HPLC-purifications used water (A) and MeCN (B) as eluents, unless otherwise stated. HPLC system A consisted of two Shimadzu LC-20AD pumps, a Shimadzu SPD-M20A diode array detector (Shimadzu Corporation, Kyoto, Japan) and NaI(Tl) radiodetector 925-SCINT (Ortec, Oak Ridge, TN, USA). The HPLC method A1 used analytical μBondapak C_{18}-column (10 μm, 125 Å, 3.9 mm × 300 mm, Waters Corporation, Milford, MA, USA) and gradient elution starting from B = 40–50% (0–5 min), 50–60% (5–6 min), 60–70% (6–7 min), 70–80% (7–8 min), 80% (8–15 min), 80–40% (15–17 min), 40% (17–22 min), flow rate 1.0 mL/min. The HPLC method A2 used analytical Kinetex PFP-column (2.6 μm,

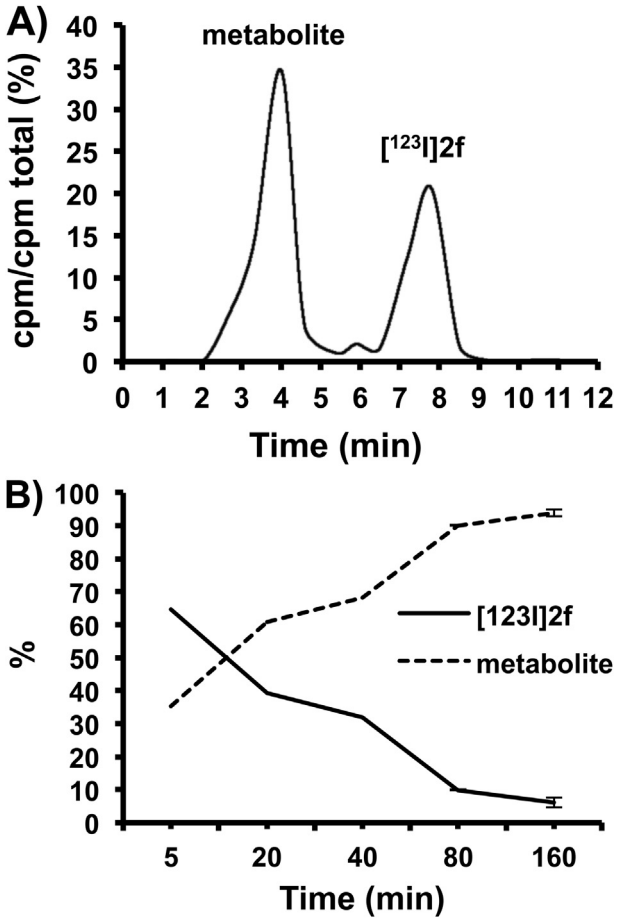

Fig. 5. (A) HPLC-chromatogram of the plasma sample at 20 min post injection of [^{123}I]**2f**. (B) The ratio of the free parent compound [^{123}I]**2f** to the main metabolite in plasma over time.

100 Å, 4.60 mm × 150 mm, Phenomenex, Torrance, CA, USA) and isocratic elution. The HPLC-method A3 used semipreparative μBondapak C_{18}-column (10 μm, 125 Å, 7.8 mm × 300 mm, Waters) and gradient elution starting from B = 30% (0–0.3 min), 30–60% (0.3–4 min), 60% (4–7 min), 60–80% (7–10 min), 80% (10–11 min), 80–30% (11–14 min), 30% (14–17 min), flow rate 4.0 mL/min. HPLC system B consisted of two Hitachi LaChrom L-7100 pumps (Hitachi Ltd., Tokyo, Japan) with Rheodyne 7010 injector, LKB 2151 UV-detector (LKB, Bromma, Sweden) and PIN diode radiodetector. The HPLC-method B1 used semipreparative μBondapak C_{18}-column (10 μm, 125 Å, 7.8 mm × 300 mm, Waters) and isocratic elution of B = 33%, flow rate 4.5 mL/min. All animal experiments were performed according to European Community Guidelines for animal experimentation and approved by the Finnish National Board of Animal Experiments.

4.2. Chemistry

4.2.1. 4-(4-Iodophenyl)butanoyl-L-proline (**4**)

4-(4-Iodophenyl)butanoic acid (**3**) (1.0 g, 3.5 mmol) was dissolved in $SOCl_2$ (1.3 mL, 17 mmol) and reacted for 2 h at 65 °C. Excess $SOCl_2$ was evaporated under reduced pressure after the reaction. The resulting 4-(4-iodophenyl)butanoyl chloride was dissolved in a small volume of diethyl ether and slowly added to a solution of Na_2CO_3 (0.93 g, 8.8 mmol) and L-proline (0.40 g, 3.5 mmol) in water (6.6 mL) at 0 °C under vigorous stirring. The mixture was stirred vigorously overnight at room temperature. The aqueous layer was washed with diethyl ether, then acidified using 2 M HCl, and extracted three times with diethyl ether. The combined diethyl ether phases from the extractions were dried with anhydrous Na_2SO_4 and evaporated under reduced pressure yielding **4** (0.98 g, 2.6 mmol, 74%). M.p. 108 °C. ^{1}H NMR (300 MHz, $CDCl_3$) δ/ppm 9.97 (br s, COOH, 1H), 7.60 (d, ArH, $^3J_{H,H}$ = 8.1 Hz, 2H), 6.94 (d, ArH, $^3J_{H,H}$ = 8.1 Hz, 2H), 4.61–4.55 (m, NCHCOO, 1H), 3.53–3.30 (m, NCH_2CH_2, 2H), 2.64 (t, $PhCH_2CH_2$, $^3J_{H,H}$ = 7.4 Hz, 2H), 2.50–1.84 (m, 2×$CH_2CH_2CH_2$; CH_2CH_2CH; CH_2CH_2CO, 8H). ^{13}C NMR (75 MHz, $CDCl_3$) δ/ppm 174.35 (COO), 173.41 (CON), 141.23 ($ArCCH_2$), 137.42 (ArCH, 2C), 130.68 (ArCH, 2C), 91.03 (ArCI), 59.31 (NCHCO), 47.50 (NCH_2CH_2), 34.48 ($PhCH_2$), 33.29 ($COCH_2$), 28.45 (CH_2CH_2CH), 25.78 ($CH_2CH_2CH_2$), 24.71 ($CH_2CH_2CH_2$).

4.2.2. 4-(4-Iodophenyl)butanoyl-L-prolyl-pyrrolidine (***2e***)

A solution of pivaloyl chloride (0.097 mL, 0.79 mmol) in DCM (0.6 mL) was slowly added to a solution of **4** (0.30 g, 0.79 mmol) and Et_3N (0.12 mL, 0.86 mmol) in DCM (1.7 mL) under argon at 0 °C. After 1 h at 0 °C a solution of Et_3N (0.12 mL, 0.86 mmol) and pyrrolidine (0.066 mL, 0.79 mmol) in DCM (0.6 mL) was added. The reaction mixture was allowed warm to room temperature and react overnight. DCM had to be added to dissolve precipitation that had formed. The solution was washed once with water, twice with saturated aqueous $NaHCO_3$ and once with water. The organic phase was dried with anhydrous Na_2SO_4 and the solvent was evaporated under reduced pressure. Flash chromatography (5% MeOH in EtOAc) gave **2e** (0.28 g, 0.64 mmol, 81%). M.p. 81 °C. $[\alpha]_{25}D = +10.5°$ (c 1.0, toluene). ^{1}H NMR (300 MHz, $CDCl_3$) δ/ppm 7.57 (d, ArH, $^3J_{H,H}$ = 8.4 Hz, 2H), 6.95 (d, ArH, $^3J_{H,H}$ = 8.4 Hz, 2H), 4.63 (dd, NCHCO, $^3J_{H,H}$ = 8.4 Hz, $^3J_{H,H}$ = 4.0 Hz, 1H), 3.81 (m, $NCH_2CH_2CH_2CHCO$, 1H), 3.59 (m, $NCH_2CH_2CH_2CHCO$ and $NCH_2CH_2CH_2CH_2$, 2H), 3.40 (m, $NCH_2CH_2CH_2CH_2$; NCH_2CH_2, 3H), 2.61 (t, $PhCH_2CH_2$, $^3J_{H,H}$ = 7.5 Hz, 2H), 1.77–2.39 (m, $CHCH_2CH_2$; CH_2CH_2CO; 4×$CH_2CH_2CH_2$, 12H). ^{13}C NMR (75 MHz, $CDCl_3$) δ/ppm 171.80 (CON), 170.90 (CON), 141.80 ($ArCCH_2$), 137.64 (ArCH, 2C), 131.04 (ArCH, 2C), 91.18 (ArCI), 58.15 (NCHCO), 47.68 (NCH_2CH_2, 2C), 34.92 (NCH_2), 33.55 ($PhCH_2$), 29.15 ($COCH_2$), 26.11 ($CH_2CH_2CH_2$; CH_2CH_2CH, 2C), 25.12 (3×$CH_2CH_2CH_2$, 3C). ESI-MS m/z = 463.2 $[M+Na]^+$. HPLC system A, method A2, solvent B = 33%, flow rate 1.15 mL/min, λ = 254 nm, t_r = 10.27 min (>99%). Calc.: C 51.81%, H 5.72%, N 6.36% Found: C 51.89%, H 5.77%, N 6.28%.

Table 2
Radioactivity in blood after i.v. injection of [^{123}I]**2f** in baseline (A) and after pretreatment with **2d** (B) at 20, 40, 80 and 160 min timepoints (n = 3). Distribution of radioactivity in different blood components in the conditions A and B is presented as percentage of the total activity in the blood after injection of [^{123}I]**2f**.

Time (min)	20		40		80		160	
Condition	A	B	A	B	A	B	A	B
Blood (%ID/g)	8.5 ± 4.0	10.9 ± 4.9	7.6 ± 4.8	4.0 ± 1.6	2.1 ± 0.9	2.7 ± 0.7	2.1 ± 0.9	1.0 ± 0.2
Unbound (%)	3[a]	47[a]	8 ± 2[b]	nd	15 ± 2[b]	nd	26 ± 7[b]	58[a]
Cell bound (%)	95[a]	53[a]	90 ± 0[b]	nd	84 ± 0[b]	nd	73 ± 6[b]	42[a]
Protein bound (%)	2[a]	0[a]	2 ± 1[b]	nd	1 ± 1[b]	nd	1 ± 2[b]	0[a]

[a] n = 1.
[b] n = 2.

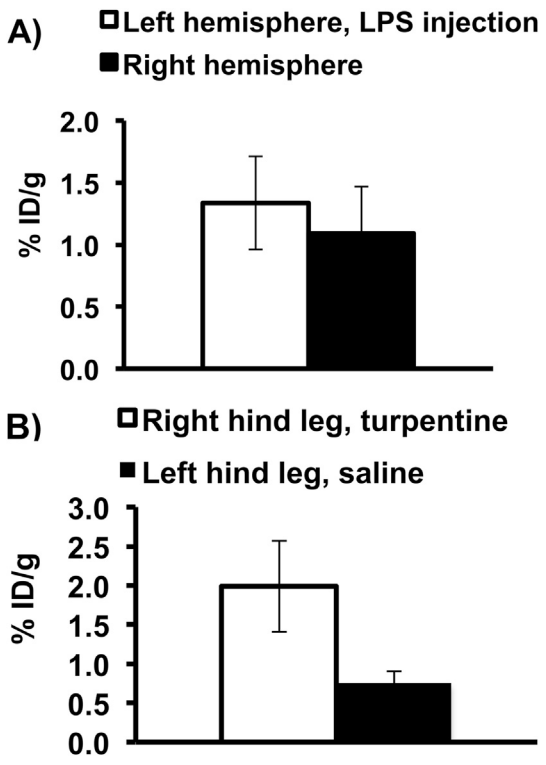

Fig. 6. The uptake of radioactivity in left and right brain hemispheres at 80 min post i.v. injection of tracer [^{123}I]**2f** administered at 24 h after LPS injection in left striatum of C57Bl/6JRccHsd male mouse (A). The uptake of radioactivity in right and left *m. gastrocnemius* at 24 h post i.v. injection of radiotracer [^{123}I]**2f** administered at 24 h after turpentine (5 μL, i.m.) injection to right hind leg of C57Bl/6JRccHsd male mouse (B).

4.2.3. 4-(4-Iodophenyl)butanoyl-L-prolyl-2(S)-cyanopyrrolidine (*2f*)

Boc-2(*S*)-cyanopyrrolidine was synthesized according to a literature procedure [39]. TFA (20 mL, 260 mmol) was added dropwise to a solution of Boc-2(*S*)-cyanopyrrolidine (0.99 g, 5.0 mmol) in DCM (60 mL) under argon at 0 °C. After 2 h 20 min the solvent was evaporated yielding the TFA salt of 2(*S*)-cyanopyrrolidine, which was used directly in the reaction below.

A solution of pivaloyl chloride (0.31 mL, 2.5 mmol) in DCM (5 mL) was slowly added to a solution of **4** (0.98 g, 2.5 mmol) and DIPEA (0.49 mL, 2.8 mmol) in DCM (50 mL) under argon at 0 °C. After 1 h at 0 °C a solution of DIPEA (2.9 mL, 17 mmol) in a small volume of DCM was added. Directly after this, a solution of the TFA salt of 2(*S*)-cyanopyrrolidine in a small volume DCM was added. The reaction mixture was allowed warm to room temperature and react overnight. The reaction mixture was diluted with DCM and washed three times with 10% aqueous citric acid, once with brine and twice with 10% aqueous $NaHCO_3$. The organic phase was dried using anhydrous Na_2SO_4 and the solvent was evaporated. Flash chromatography (1% MeOH in DCM) yielded **2f** (670 mg, 1.4 mmol, 57%). M.p. 128 °C. $[\alpha]_{25}D = -71.9°$ (c 1.0, CHCl3). ^{1}H NMR (300 MHz, $CDCl_3$) δ/ppm 7.58 (d, ArH, $^3J_{H,H}$ = 8.3 Hz, 2H), 6.94 (d, ArH, $^3J_{H,H}$ = 8.3 Hz, 2H), 4.81 (m, NCHCO, 1H), 4.55 (dd, NCHCN, $^3J_{H,H}$ = 8.1 Hz, $^3J_{H,H}$ = 4.0 Hz, 1H), 3.86 (m, $NCH_2CH_2CH_2CHCO$, 1H), 3.62 (m, $NCH_2CH_2CH_2CHCO$, 1H), 3.62 (m, $NCH_2CH_2CH_2CHCN$, 1H), 3.44 (dt, $^2J_{H,H}$ = 13.6 Hz, $^3J_{H,H}$ = 7.0 Hz, $NCH_2CH_2CH_2CHCN$, 1H), 2.60 (t, $PhCH_2CH_2$, $^3J_{H,H}$ = 7.1 Hz, 2H), 2.22 (m, CH_2CH_2CO; (CN)$CHCH_2CH_2$; (CO)$CHCH_2CH_2$; $PhCH_2CH_2CH_2$, 8H), 1.95 (m, $NCH_2CH_2CH_2$, 4H). ^{13}C NMR (75 MHz, $CDCl_3$) δ/ppm 171.75 (CON), 171.59 (CON),141.64 ($ArCCH_2$), 137.67 (ArCH, 2C), 130.98 (ArCH, 2C), 118.92 (CN), 91.23 (ArCI), 57.75 (NCHCO), 47.60 (NCHCN), 46.83 (NCH_2), 46.66 (NCH_2), 34.87 ($COCH_2$), 33.55 ($PhCH_2$), 30.02 ($CNCHCH_2$), 29.03 ($COCHCH_2$), 26.05 ($PhCH_2CH_2CH_2$), 25.69 ($NCH_2CH_2CH_2$), 25.19 ($NCH_2CH_2CH_2$). ESI-MS m/z = 488.3 $[M+Na]^+$. HPLC system A, method A2, solvent B = 33%, flow rate 1.15 mL/min, λ = 254 nm, t_r = 10.65 min (>99%). Calc.: C 51.62%, H 5.20%, N 9.03% Found: C 51.83%, H 5.46%, N 8.81%.

4.2.4. 4-(4-Trimethylstannylphenyl)butanoyl-L-prolyl-pyrrolidine (*5a*)

To a solution of iodide (**2e**) (30 mg, 0.069 mmol) in toluene (1.0 mL) were added hexamethylditin (57 μL, 0.276 mmol in toluene 0.3 mL) and $Pd(PPh_3)_4$ (8.3 mg, 0.007 mmol in toluene 1.0 mL). After being refluxed at 110 °C for 3 h, reaction mixture was cooled down to room temperature and filtered through a pad of celite. The filtrate was concentrated under reduced pressure to give oily crude product. Column chromatography on silica gel (EtOAc) gave **5a** as colorless oil (24 mg, 0.050 mmol, 73%). $[\alpha]_{25}D = +116.3°$ (c 0.05, MeCN). ^{1}H NMR (300 MHz, $CDCl_3$) δ/ppm 7.39 (d, ArH, $^3J_{H,H}$ = 7.9 Hz, 2H), 7.18 (d, ArH, $^3J_{H,H}$ = 7.9 Hz), 4.63 (dd, $^3J_{H,H}$ = 8.4 Hz, $^3J_{H,H}$ = 3.7 Hz, NCHCO, 1H), 3.83 (m, $NCH_2CH_2CH_2CHCO$, 1H), 3.50–3.70 (m, $NCH_2CH_2CH_2CHCO$, 2H), 3.29–3.48 (m, $NCH_2CH_2CH_2CH_2$, 3H), 2.65 (t, $PhCH_2CH_2$, $^3J_{H,H}$ = 7.4 Hz, 2H), 2.30 (m, CH_2CH_2CHCO, 2H), 1.73–2.26 (m, 4×$CH_2CH_2CH_2$, CH_2CH_2CO, 10H), 0.26 (s, $(CH_3)_3Sn$, 9H). ^{13}C NMR (75 MHz, $CDCl_3$) δ/ppm 171.73 (CH_2CON), 171.03 (CHCON), 142.19 (ArCH), 139.19 ($ArCCH_2$), 136.12 ($ArCSn(CH_3)_3$), 128.71 (ArCH), 57.94 (NCHCO), 47.53 (NCH_2), 46.60 (NCH_2), 46.23 (NCH_2), 35.45 (CH_2CO), 33.92 ($PhCH_2$), 29.16 ($CHCH_2CH_2$), 26.50 ($CH_2CH_2CH_2$), 26.14 ($CH_2CH_2CH_2$), 25.10 ($CH_2CH_2CH_2$), 24.44 ($CH_2CH_2CH_2$), −9.28 (($CH_3)_3Sn$). ESI-MS m/z = 501.3 $[M+Na]^+$. HPLC system A, method A2, solvent B = 45%, flow rate 1.2 mL/min, λ = 220 nm, t_r = 7.65 min (86%).

4.2.5. 4-(4-Trimethylstannylphenyl)butanoyl-L-prolyl-2(S)-cyanopyrrolidine (*5b*)

Compound **5b** was synthesized and purified as above using **2f** as starting material. Purification gave **5b** as colorless oil (75%). $[\alpha]_{25}D = -103.5°$ (c 0.05, MeCN). ^{1}H NMR (300 MHz, $CDCl_3$) δ/ppm 7.40 (d, ArH, $^3J_{H,H}$ = 7.9 Hz, 2H), 7.17 (d, ArH, $^3J_{H,H}$ = 7.9 Hz, 2H), 4.83 (m, NCHCO, 1H), 4.56 (dd, $^3J_{H,H}$ = 8.1 Hz, $^3J_{H,H}$ = 4.0 Hz, NCHCN, 1H), 3.89 (m, $NCH_2CH_2CH_2CHCO$, 1H), 3.63 (m, $NCH_2CH_2CH_2CHCO$, 1H), 3.63 (m, $NCH_2CH_2CH_2CHCN$, 1H), 3.45 (dt, $^2J_{H,H}$ = 9.7 Hz, $^3J_{H,H}$ = 7.0 Hz, $NCH_2CH_2CH_2CHCN$, 1H), 2.64 (t, $PhCH_2CH_2$, $^3J_{H,H}$ = 7.5 Hz, 2H), 2.22 (m, CH_2CH_2CO; (CN)$CHCH_2CH_2$; (CO)$CHCH_2CH_2$; $PhCH_2CH_2CH_2$, 8H), 1.96 (m, $NCH_2CH_2CH_2$, 4H), 0.25 (s, $(CH_3)_3Sn$, 9H). ^{13}C NMR (75 MHz, $CDCl_3$) δ/ppm 172.04 ($CH_2(CO)N$), 171.69 (CH(CO)N), 141.98 ($ArCCH_2$), 139.36 (ArCSn), 136.17 (ArCH, 2C), 128.67 (ArCH, 2C), 118.96 (CN), 57.69 (NCHCO), 47.57 (NCHCN), 46.83 (NCH_2), 46.66 (NCH_2), 35.37 ($COCH_2$), 33.81 ($PhCH_2$), 30.00 ($CNCHCH_2$), 29.04 ($COCHCH_2$), 26.15 ($PhCH_2CH_2CH_2$), 25.68 ($CH_2CH_2CH_2$), 25.19 ($CH_2CH_2CH_2$), −9.27 (($CH_3)_3Sn$, 3C). ESI-MS m/z = 526.3 $[M+Na]^+$. HPLC system A, method A2, solvent B = 45%, flow rate 1.2 mL/min, λ = 220 nm, t_r = 10.29 (92%).

4.2.6. Evaluation of the binding properties with in vitro enzyme assay

The effect of **2e** and **2f** on the enzymatic cleavage of benzyloxycarbonyl-glycyl-alanyl-prolyl-7-amino-4-methyl-coumarine (Z-Gly-Ala-Pro-AMC) by POP, to free the fluorescent AMC, was performed by monitoring the fluorescence change on a reader (Victor-2, PerkinElmer, Waltham MA, USA). Reactions were performed at 37 °C for 60 min in a 96-well plates in a final volume of 100 μL which contained 0.2, 0.5 or 1 mM Z-Gly-Pro-AMC, 10 fmol of recombinant porcine POP, in assay buffer (75 mM phosphate buffer pH = 7, and 5 mM DTT), in the absence or presence of increasing concentrations of the parent KYP-2047 or iodinated compounds

(0.5 nM–1 mM). The reaction was stopped by adding 100 μL of ammonium acetate (1 M, pH = 4). Fluorescence was read at excitation λ 360 nm and emission λ 460 nm. Fluorescence values were interpolated on an AMC standard curve (0.5–10 nmol AMC in 100 μL of assay buffer). Background fluorescence of the amounts used of Z-Gly-Ala-Pro-AMC were subtracted. K_i was determined from the intercepts in the double reciprocal plots of data fitted by linear regression of the mean of the activities (triplicate), at every condition, using data of three independent experiments.

4.3. Radiochemistry

Radioiodine labeling solution [^{123}I]NaI (in 0.1 M NaOH) was a product of MAP Medical Technologies Oy (Helsinki, Finland). The specific activity of the labeling solution was 1.3*10–35 TBq/mg and the radionuclidic purity >99.8% (^{123}I). Human plasma was obtained from the Finnish Red Cross Blood Service (Helsinki, Finland). Synthesis, purification and formulation were conducted in lead shielded hot cells. The separation and purification of the tracer was performed on the HPLC system B using method B1. The analyses of the radioactive purity and specific activity were performed on the HPLC system A using methods A1 and A2, respectively. The analyses of the radioactive metabolites were performed on HPLC system A using method A3. For the gamma-activity counting of the biological samples Wizard 3″ 1480 gammacounter (PerkinElmer, Waltham, MA, USA) was used. Digital autoradiography of tissue sections was based on photostimulated luminescence detection on a Fujifilm FLA-5100 system and Image Reader FLA-5000 series v1.0 software (Fujifilm, Tokyo, Japan). The autoradiography data was processed using AIDA Image Analyzer v.4.00 program (Raytest Isotopen messgeräte GmbH, Straubenhardt, Germany). SPECT-CT imaging was carried out with NanoSPECT/CT (Bioscan Inc., Washington, DC, USA).

4.3.1. 4-(4-[^{123}I]iodophenyl)butanoyl-L-prolyl-pyrrolidine ([^{123}I]**2e**)

The small-scale radiosynthesis of [^{123}I]**2e** (starting activity 10 MBq) was performed starting from the precursor **5a** following the method described below for the tracer [^{123}I]**2f** that was selected for *in vivo* studies. The HPLC system B, method B1 (MeCN/H_2O, 33%; 4.5 mL/min; μBondapak C-$_{18}$ column, 7.8 × 300 mm; λ = 220 nm, Waters) was used for the purification of the product [^{123}I]**2e** (t_r = 17.5 min). The decay corrected, isolated radiochemical yield and the radiochemical purity of [^{123}I]**2e** were >99% and >99%, respectively.

4.3.2. 4-(4-[^{123}I]iodophenyl)butanoyl-L-prolyl-2(S)-cyanopyrrolidine ([^{123}I]**2f**)

To a glass vial, 0.1 mg (0.2 μmol) of precursor **5b** was added in a small amount of ethanol (0.1 mL). HCl (90 μL, 0.05 M) was added, followed by the addition of [^{123}I]NaI-labeling solution (90 μL, 0.05 M NaOH, 300–680 MBq). After this, peracetic acid solution was added to the vial (8 μL, 3.9% in water) and the reaction solution was mixed gently and let to react for 10 min at room temperature. Sodium metabisulphite (160 μL, 2.85 mg/mL) was added to quench the remaining unreacted oxidant. The reaction solution was diluted with water (2 mL) and the resulting mixture was purified by using the HPLC system B, method B1 (MeCN/H_2O, 33%; 4.5 mL/min; μBondapak C-$_{18}$ column, 7.8 × 300 mm; λ = 220 nm, Waters). The product fraction (t_r = 21 min) was collected, diluted with water (up to 20 mL), and the resulting solution was passed through a C-$_{18}$ SPE cartridge (Sep-Pak® Plus C18, Waters). The product was eluted out with ethanol (1.5 mL) and evaporated to dryness under reduced pressure. The resulting product was re-dissolved in a solution of DMSO (1%) in 0.9% NaCl (v/v). The product [^{123}I]**2f** was obtained with radiochemical incorporation yield of 87 ± 4% in 133 ± 33 min. The radiochemical purity of the tracer [^{123}I]**2f** was >99% at the end of synthesis, and 98.9 ± 2% after 24 h. Specific activity was 456 ± 98 GBq/μmol at the end of synthesis.

4.3.3. Determination of the partition coefficient (LogP)

Lipophilicity of [^{123}I]**2f** was assessed by the determination of the partition of the compound between water and *n*-octanol phases following a method described in the literature [27]. Briefly, [^{123}I]**2f** (40 μL, 1% DMSO in 0.9% NaCl, 700 kBq) was added to the mixture of phosphate buffer (10 mL, 0.02 M, pH 7.4) and *n*-octanol (10 mL) in a separation funnel. The mixture was shaken for 3 min, after which the aqueous phase was discarded. The octanol phase was pipetted to four test tubes (2 mL to each) and equal amount of phosphate buffer (0.02 M, pH 7.4) was added to each tube. The mixtures were shaken for 10 min and centrifuged for 5 min at 1000 g. Samples from the aqueous (0.5 mL) and octanol (0.5 mL) phases were taken from each test tube for the activity measurement with γ-counter (PerkinElmer Wizard, 120 s). The partition coefficient was determined by calculating the logarithm of the ratio (cpm/mL in octanol)/(cpm/mL in buffer) from the four replicates, and the data was expressed as mean value ± standard deviation.

4.3.4. In vitro stability in human plasma

Plasma stability of [^{123}I]**2f** was determined by incubation in human plasma at 37 °C for up to 120 min. The tracer (5 MBq) was formulated in PBS (2.0 mL) and this solution was divided equally into 5 eppendorf tubes each containing human plasma (400 μL). After incubation (15, 30, 60, 90 and 120 min) at 37 °C, the proteins were precipitated with MeCN (600 μL) and the mixture was centrifuged for 5 min at 10 000 *g*. The supernatant was collected carefully and the activities of ^{123}I in pellet and supernatant were measured. The supernatant was analyzed with HPLC system A using gradient method A3 (t_r parent = 7.68 min).

4.3.5. Plasma metabolites in mouse

3.6 MBq of [^{123}I]**2f** was administered to C57Bl/6JRccHsd male mice via the lateral tail vein. The animals were sacrificed at 5, 20, 40, 80 and 160 min post injection. Blood samples were immediately obtained via cardiac puncture with heparin wetted syringe and placed on ice. Similarly, blood samples were taken from the mice pretreated with **2d** (KYP-2047, 50 μmol/kg, 10 mL/kg, DMSO (1%) in NaCl (0.9%)). The sample was weighed and a small aliquot was taken for the gamma-activity measurement (PerkinElmer Wizard γ-counter, 120 s). The rest of the blood was centrifuged for 5 min at 2000 g to separate plasma and the blood cells. The weight of the plasma was measured, and a small aliquot of the plasma was taken for the activity measurements. Acetonitrile (1.5 × the volume of plasma) was added to the residual plasma and the mixture was centrifuged for 5 min at 2000 g. Again, the supernatant was weighed and an aliquot of the supernatant was taken for γ-measurement. On the basis of these results, the binding of the tracer to plasma proteins and blood cells was calculated. The rest of the supernatant was analyzed by HPLC system A, gradient method A3. Fractions of 0.65 min were collected and the activities were measured with a γ-counter.

4.4. Animal experiments

4.4.1. Biodistribution

C57Bl/6JRccHsd male mice (aged 8–12 weeks, 18–29 g) were anesthetized with isoflurane (IsoFlo® vet, Orion Pharma, Espoo, Finland) in medical oxygen carrier (4% for induction at 4 L/min, 2% for upkeep at 2–3 L/min) and the lateral tail vein was cannulated using a temporary catheter fabricated out of a 30G needle and a PE10 polyethylene tubing (AgnTho's, Lidingö, Sweden). [^{123}I]**2f**

(dose 2.86 ± 1.26 MBq/mouse) in 1% DMSO in 0.9% NaCl was injected as a bolus (an average of 65 μL of compound flushed with 60 μL of saline) via tail vein. For the determination of non-specific binding of the tracer, KYP-2047 (50 μmol/kg, 10 mL/kg, in DMSO (1%)/0.9% NaCl) was injected i.p. 10 min prior to tracer administration. Animals were sacrificed at 5, 20, 40, 80 and 160 min after administration.

4.4.2. Animal models

LPS induced acute neuroinflammation model. C57BL/6JRccHsd male mice were deeply anaesthetized with isoflurane (2–4%) and placed in a stereotaxic frame (Stoelting, Wood Dale, IL, USA). Each mouse received a stereotaxic microinjection of a 2 μL solution containing 5 μg LPS (*Escherichia coli* serotype 055:B5, Sigma–Aldrich, St. Louis, MO, USA) into the left striatum 24 h prior to administration of [^{123}I]**2f**. The injections were done using a 10 μL Hamilton-microsyringe connected to an injector (Stoelting) at 0.5 μL/min to the coordinates A/P +0.7; M/L +1.8; D/V −2.7. After the injection, the needle was kept in place for an additional 4 min and then slowly retracted to prevent reflux. Mice received buprenorphine (0.1 mg/kg, s.c., Temgesic®, Reckitt Benckiser Healthcare (UK) Ltd, East Yorkshire, Great Britain) for post-operative pain relief, and were single-housed after the operation. The right hemisphere of the mice were left intact and served as a control for LPS-induced inflammation.

Turpentine induced model of acute localized inflammation. C57BL/6JRccHsd male mice were anaesthetized with isoflurane in air carrier (4% for induction, 2% for upkeep). The injection area was carefully shaved with a scalpel blade and disinfected with iodine solution. Turpentine oil (5 μL) was injected i.m. into *m. gastrocnemius* in the right hind leg with a 30G needle. Saline (0.9%, 5 μL) was injected i.m. into the same area in the left hind leg as a control. The pain due to operation was alleviated with Temgesic® (0.1 mg/kg, 0.015 mg/mL in 0.9% NaCl, s.c.), administered in every 12 h until the SPECT/CT scan.

4.4.3. Small animal SPECT scanning

C57Bl/6JRccHsd male mice (aged 8–12 weeks, 18–29 g) were anesthetized with isoflurane (4% for induction, 2% for upkeep) in either air (injection) or 0.8 L/min medical oxygen (imaging) as the carrier gas. A dose of 47.6 ± 4.1 MBq of [^{123}I]**2f** in 100 μL was administered intravenously by cannula 30G temporary catheter, after which the cannula was flushed with 100 μL of 0.9% NaCl solution. Radioactivity in the syringe was measured prior to and post-injection with dose calibrator (CRC-25R, Capintec Inc., Ramsey, NJ, USA). For the blocking studies, mice received i.p. injection of **2d** (KYP-2047) 10 min prior to tracer administration as above.

SPECT-CT imaging was carried out with NanoSPECT/CT (Bioscan Inc., USA), a four-headed small animal scanner featuring 1.0 mm multipinhole mouse apertures. The body temperature of mice was maintained warm throughout the study by using a temperature-controlled animal bed (Minerve, France). Brain SPECT images were acquired 20 min, 40 min and 60 min post-injection in 24 projections using time per projection of 200 s resulting in acquisition time of 20 min/scan. Alternatively, mice were imaged only once starting 20 min post-injection by using time per projection of 600 s and total acquisition time of 60 min. CT imaging was performed with 45 kVp tube voltage in 180 projections. SPECT images were reconstructed with HiSPECT NG software (Scivis GmbH, Göttingen, Germany) and fused with CT datasets with InVivoScope software (Bioscan Inc., USA).

To quantify tracer uptake in brain areas, reconstructed SPECT images were reoriented and analyzed with InVivoScope (Bioscan Inc., USA) software by using CT data as a reference. Three-dimensional volumes of interest (VOIs) were defined to cover whole brain region, right side, and left side by using 3D ROI tool. The VOIs were saved and used for all subsequent analyses. The radioactivity in each VOI was calculated and results are presented as a percentage from injected dose.

Acknowledgments

Academy of Finland (Grant Nos. 136805 and 140965), the Finnish funding agency for technology and innovation (TEKES grant No. 40044/11) and FinPharma Doctoral Program (drug discovery section) are acknowledged for the financial support.

References

[1] A.J. Barret, N.D. Rawlings, Families and clans in serine peptidases, Archives of Biochemistry and Biophysics 318 (1995) 247–250.
[2] N.D. Rawlings, L. Polgar, A.J. Barret, A new family of serine-type peptidases related to prolyl oligopeptidase, Biochemical Journal 279 (1991) 907–911.
[3] J. Tenorio-Laranga, J.I. Venäläinen, P.T. Männistö, J.A. García-Horsman, Characterization of membrane-bound prolyl endopeptidase from brain, FEBS Journal 275 (2008) 4415–4427.
[4] J.A. García-Horsman, P.T. Männistö, J.I. Venäläinen, On the role of prolyl oligopeptidase in health and disease, Neuropeptides 41 (2007) 1–24.
[5] A.J. Jalkanen, K. Savolainen, M.M. Forsberg, Inhibition of prolyl oligopeptidase by KYP-2047 fails to increase the extracellular neurotensin and substance P levels in rat striatum, Neuroscience Letters 502 (2011) 107–111.
[6] R.S.B. Williams, M. Eames, W.J. Ryves, J. Viggars, A.J. Harwood, Loss of prolyl oligopeptidase confers resistance to lithium by elevation of inositol (1,4,5) trisphosphate, EMBO Journal 18 (1999) 2734–2745.
[7] I. Brandt, M. Gérard, K. Sergeant, B. Devreese, V. Baekelandt, K. Augustyns, S. Scharpé, Y. Engelborghs, A.-M. Lambeir, Prolyl oligopeptidase stimulates the aggregation of α-synuclein, Peptides 29 (2008) 1472–1478.
[8] A.-M. Lambeir, Interaction of prolyl oligopeptidase with α-synuclein, CNS & Neurological Disorders – Drug Targets 10 (2011) 349–354.
[9] T.T. Myöhänen, M.J. Hannula, R. Van Elzen, M. Gerard, P. Van Der Veken, J.A. García-Horsman, V. Baekelandt, P.T. Männistö, A.-M. Lambeir, A prolyl oligopeptidase inhibitor, KYP-2047, reduces α-synuclein protein levels and aggregates in cellular and animal models of parkinson's disease, British Journal of Pharmacology 166 (2012) 1097–1113.
[10] M.J. Hannula, T.T. Myöhänen, J. Tenorio-Laranga, P.T. Männistö, J.A. García-Horsman, Prolyl oligopeptidase colocalizes with α-synuclein, β-amyloid, tau protein and astroglia in the post-mortem brain samples with Parkinson's and Alzheimer's diseases, Neuroscience 242 (2013) 140–150.
[11] A. Penttinen, J. Tenorio-Langa, A. Siikanen, M. Morawski, S. Roßner, J.A. García-Horsman, Prolyl oligopeptidase: a rising star on the stage of neuroinflammation research, CNS & Neurological Disorders – Drug Targets 10 (2011) 340–348.
[12] P. O'Reilly, M.T. Hardison, P.L. Jackson, X. Xu, R.J. Snelgrove, A. Gaggar, F.S. Galin, J.E. Blalock, Neutrophils contain prolyl endopeptidase and generate the chemotactic peptide, PGP, from collagen, Journal of Neuroimmunology 217 (2009) 51–54.
[13] J. Tenorio-Laranga, I. Peltonen, S. Keskitalo, G. Duran-Torres, R. Natarajan, P.T. Männistö, A. Nurmi, N. Vartiainen, L. Airas, I. Elovaara, J.A. García-Horsman, Alteration of prolyl oligopeptidase and activated a-2-macroglobulin in multiple sclerosis subtypes and in the clinically isolated syndrome, Biochemical Pharmacology 85 (2013) 1783–1794.
[14] J. Tenorio-Laranga, F. Coret-Ferrer, B. Casanova-Estruch, M. Burgal, J.A. García-Horsman, Prolyl oligopeptidase is inhibited in relapsing-remitting multiple sclerosis, Journal of Neuroinflammation 7 (2010) 23.
[15] J.I. Venäläinen, E.A.A. Wallén, A. Poso, J.A. García-Horsman, P.T. Männistö, Synthesis and characterization of the novel fluorescent prolyl oligopeptidase inhibitor 4-fluoresceinthiocarbamoyl-6-aminocaproyl-L-prolyl-2(*S*)-(hydroxyacetyl)pyrrolidine, Journal of Medicinal Chemistry 48 (2005) 7093–7095.
[16] M.-J. Moreno-Baylach, V. Felipo, P.T. Männistö, J.A. García-Horsman, Expression and traffic of cellular prolyl oligopeptidase are regulated during cerebellar granule cell differentiation, maturation, and aging, Neuroscience 156 (2008) 580–585.
[17] T. Nakajima, Y. Ono, A. Kato, J. Maeda, T. Ohe, Y-29794 – a nonpeptide prolyl endopeptidase inhibitor that can penetrate into the brain, Neuroscience Letters 141 (1992) 156–160.
[18] J.R. Atack, N. Suman-Chauhan, G. Dawson, J.J. Kulagowski, In vitro and in vivo inhibition of prolyl endopeptidase, European Journal of Pharmacology 205 (1991) 157–163.
[19] A. Charalambous, T.J. Mangner, M.R. Kilbourn, Synthesis of (N-[^{11}C]methyl) Y-29794, a competitive inhibitor of prolyl endopeptidase, Journal of Labelled Compounds and Radiopharmaceuticals 34 (1994) 499–503.
[20] M.E. Van Dort, M.R. Kilbourn, T.J. Mangner, Synthesis of N-(N-(-4-(N-[^{11}C] methylamino)phenyl)butyryl)-L-prolyl)pyrrolidine: a potential radiotracer for prolyl endopeptidase, Journal of Labelled Compounds and Radiopharmaceuticals 34 (1994) 447–452.

[21] M. Saito, M. Hashimoto, N. Kawaguchi, H. Shibata, H. Fukami, T. Tanaka, N. Higuchi, Synthesis and inhibitory activity of acyl-peptidyl-pyrrolidine derivatives toward post-proline cleaving enzyme; a study of subsite specificity, Journal of Enzyme Inhibition 5 (1991) 51–75.
[22] E.M. Jarho, J.I. Venäläinen, J. Huuskonen, J.A. Christiaans, J.A. García-Horsman, M.M. Forsberg, T. Järvinen, J. Gynther, P.T. Männistö, E.A.A. Wallén, Cyclopent-2-enecarbonyl group mimics proline at the P2 position of prolyl oligopeptidase inhibitors, Journal of Medicinal Chemistry 47 (2004) 5605–5607.
[23] J.I. Venäläinen, J.A. García-Horsman, M.M. Forsberg, A. Jalkanen, E.A.A. Wallén, E.M. Jarho, J.A.M. Christiaans, J. Gynther, P.T. Männistö, Binding kinetics and duration of in vivo action of novel prolyl oligopeptidase inhibitors, Biochemical Pharmacology 71 (2006) 683–692.
[24] K. Kaszuba, T. Róg, R. Danne, P. Canning, V. Fülöp, T. Juhász, Z. Szeltner, J.-F. St. Pierre, A. García-Horsman, P.T. Männistö, M. Karttunen, J. Hokkanen, A. Bunker, Molecular dynamics, crystallography and mutagenesis studies on the substrate gating mechanism of prolyl oligopeptidase, Biochimie 94 (2008) 1398–1411.
[25] H. Arai, H. Nishioka, S. Niwa, T. Yamanaka, Y. Tanaka, K. Yoshinaga, N. Kobayashi, N. Miura, Y. Ikeda, Synthesis of prolyl endopeptidase inhibitors and evaluation of their structure-activity relationships: in vitro inhibition of prolyl endopeptidase from canine brain, Chemical & Pharmaceutical Bulletin 41 (1993) 1583–1588.
[26] H.H. Coenen, J. Mertens, B. Mazière, Radioiodination Reactions for Pharmaceuticals, in: Compendium for Effective Synthesis Strategies, Springer, Dordrecht, The Netherlands, 2006.
[27] H. Pajouhesh, G.R. Lenz, Medicinal chemical properties of successful central nervous system drugs, NeuroRx 2 (2005) 541–553.
[28] A.A. Wilson, L. Jin, A. Garcia, J.N. DaSilva, S. Houle, An admonition when measuring the lipophilicity of radiotracers using counting techniques, Applied Radiation and Isotopes 54 (2001) 203–208.
[29] S. Wilk, Prolyl endopeptidase, Life Sciences 33 (1983) 2149–2157.
[30] T.T. Myöhänen, J.I. Venäläinen, J.A. García-Horsman, M. Piltonen, P.T. Männistö, Distribution of prolyl oligopeptidase in the mouse whole-body sections and peripheral tissues, Histochemistry and Cell Biology 130 (2008) 993–1003.
[31] A.J. Jalkanen, T.P. Piepponen, J.J. Hakkarainen, I. De Meester, A.-M. Lambeir, M. Forsberg, The effect of prolyl oligopeptidase inhibition on extracellular acetylcholine and dopamine levels in the rat striatum, Neurochemistry International 60 (2012) 301–309.
[32] H. He, P. Tran, H. Yin, H. Smith, Y. Batard, L. Wang, H. Einolf, H. Gu, J.B. Mangold, V. Fischer, D. Howard, Adsorption, metabolism, and excretion of [^{14}C]vildagliptin, a novel dipeptidyl peptidase 4 inhibitor, in humans, Drug Metabolism and Disposition 37 (2009) 536–544.
[33] V.W. Pike, PET radiotracers: crossing the blood-brain barrier and surviving metabolism, Trends in Pharmacological Sciences 30 (2009) 431–440.
[34] F. Goossens, I. De Meester, G. Vanhoof, S. Scharpé, Distribution of prolyl oligopeptidase in human peripheral tissues and body fluids, European Journal of Clinical Chemistry and Clinical Biochemistry 34 (1996) 17–22.
[35] C. Odaka, T. Mizuochi, T. Shirasawa, P. Morain, F. Checler, Murine T cells expressing high activity of prolyl endopeptidase are susceptible to activation-induced cell death, FEBS Letters 512 (2002) 163–167.
[36] R.L. Hunter, B. Cheng, D.-Y. Choi, M. Liu, S. Liu, W.A. Cass, G. Bing, Intrastriatal lipopolysaccharide injection induced Parkinsonism in C57/B6 mice, Journal of Neuroscience Research 87 (2009) 1913–1921.
[37] K.U. Tufekci, S. Genc, K. Genc, The endotoxin-induced neuroinflammation model of Parkinson's disease, Parkinsons Disease (2011) 487450.
[38] S. Aid, A.C. Silva, E. Candelario-Jalil, S.-H. Choi, G.A. Rosenberg, F. Bosetti, Cyclooxygenase-1 and -2 differentially modulate lipopolysaccharide-induced blood-brain barrier disruption through matrix metalloproteinase activity, Journal of Cerebral Blood Flow and Metabolism 30 (2010) 370–380.
[39] E.A.A. Wallén, J.A.M. Christiaans, M.M. Forsberg, J.I. Venäläinen, P.T. Männistö, J. Gynther, Dicarboxylic acid bis(L-prolyl-pyrrolidine) amides as prolyl oligopeptidase inhibitors, Journal of Medicinal Chemistry 45 (2002) 4581–4584. Supporting Info.